HHS Public Access

Author manuscript

J Magn Reson Imaging. Author manuscript; available in PMC 2022 April 23.

Published in final edited form as:

J Magn Reson Imaging. 2021 October ; 54(4): 1257–1265. doi:10.1002/jmri.27608.

Impact of Wideband Late Gadolinium Enhancement Cardiac Magnetic Resonance Imaging on Device-Related Artifacts in Different Implantable Cardioverter-Defibrillator Types

Amita Singh, MD[1], **Wensu Chen, MD**[1,2], **Hena N. Patel, MD**[1], **Nazia Alvi, DO**[1], **Keigo Kawaji, PhD**[1,3], **Stephanie A. Besser, MSAS, MSPA**[1], **Roderick Tung, MD**[1], **Jiangang Zou, MD, PhD**[2], **Roberto M. Lang, MD**[1], **Victor Mor-Avi, PhD**[1], **Amit R. Patel, MD**[1,*]

[1]Department of Medicine, Section of Cardiology, University of Chicago Medicine, Chicago, Illinois, USA

[2]Cardiology Department, First Affiliated Hospital, Nanjing Medical University, Nanjing, China

[3]Department of Biomedical Engineering, Illinois Institute of Technology, Chicago, Illinois, USA

Abstract

Background: Late gadolinium enhancement (LGE) imaging in patients with implantable cardioverter-defibrillators (ICD) is limited by device-related artifacts (DRA). The use of wideband (WB) LGE protocols improves LGE images, but their efficacy with different ICD types is not well known.

Purpose: To assess the effects of WB LGE imaging on DRA in different non-MR conditional ICD subtypes.

Study Type: Retrospective.

Population: A total of 113 patients undergoing cardiac magnetic resonance imaging with three ICD subtypes: transvenous (TV-ICD, $N = 48$), cardiac-resynchronization therapy device (CRT-D, $N = 48$), and subcutaneous (S-ICD, $N = 17$).

Field Strength/Sequence: 5 T scanner, standard LGE, and WB LGE imaging with a phase-sensitive inversion recovery segmented gradient echo sequence.

Assessment: DRA burden was defined as the number of artifact-positive short-axis LGE slices as percentage of the total number of short-axis slices covering the left ventricle from based to apex, and was determined for WB and standard LGE studies for each patient. Additionally, artifact area on each slice was quantified.

Statistical Tests: Shapiro–Wilks, Kruskal–Wallis analysis of variance, Dunn tests with Bonferroni correction, and Mann–Whitney *U*-test.

[*]Address reprint requests to: A.R.P., 5758 S. Maryland Avenue, MC9067, Chicago, IL 60637. amitpatel@uchicago.edu.

Level of Evidence: 1

Technical Efficacy: Stage: 5

Results: In patients with TV-ICD, DRA burden was significantly reduced and nearly eliminated with WB LGE compared to standard LGE imaging (median [interquartile range]: 0 [0–7]% vs. 18 [0–50]%, $P < 0.05$), but WB imaging had less of an impact on DRA in the CRT-D (8 [0–23]% vs. 16 [0–45]%, p = 0.12) and S-ICD (60 [15–71]% vs. 67 [50–92]%, $P = 0.09$) patients. Residual DRA was significantly greater ($P < 0.05$) for S-ICD compared to other device types with WB LGE imaging, despite the generators of all three ICD types having similar proximity to the heart. The area of S-ICD associated DRA was smaller with WB LGE ($P < 0.001$) than with standard LGE imaging and the artifacts had different characteristics (dark signal void instead of a bright hyperenhancement artifact).

Data Conclusion: Although WB LGE imaging reduced the burden of DRA caused by S-ICD, the residual artifact was greater than that observed with TV-ICD and CRT-D devices. Further developments are needed to better resolve S-ICD artifacts.

Introduction

There is a growing body of data to support both the safety and feasibility of thoracic magnetic resonance imaging (MRI) in patients with pre-existing, non-MR conditional implantable cardioverter-defibrillator (ICD) devices.[1, 2] Contemporaneously with other groups, we have reported on image quality improvement in cardiac MRI using wideband (WB) late gadolinium enhancement (LGE) imaging sequences for the assessment of myocardial fibrosis or scar.[3–6] The presence of an ICD leads to magnetic field inhomogeneity, which in standard LGE imaging, causes typical device-related artifacts (DRA), including signal void, susceptibility and off-resonance artifacts. The latter occur due to the proximity of regions of myocardium and other cardiac structures to the ICD components, causing a resonant frequency shift, which may give the spurious appearance of hyperenhancement on standard LGE sequences, and be falsely interpreted as myocardial fibrosis. WB LGE imaging employs a larger bandwidth for the inversion pulse applied during LGE imaging, which can diminish the severity and extent of hyperenhancement artifacts. In addition to significant reductions in DRAs with WB LGE imaging, scar detection from WB LGE images has been shown to correlate well with invasive electroanatomic mapping of myocardial scar across a spectrum of pathologies.[6, 7]

The utility of WB LGE imaging has predominantly been studied in patients with traditional transvenous devices (TV-ICD), and less is known about its effectiveness in patients with other ICD subtypes. These include ICDs for cardiac resynchronization therapy (CRT-D), which involve an additional pacing lead in the coronary sinus, and subcutaneous ICDs (S-ICD), which were approved for clinical use within the last 10 years.[8] Compared to conventional TV-ICD systems, in which the pulse generator pocket is placed in the upper chest, the S-ICD pulse generator pocket is typically in the left mid-axillary line, with a lead tunneled in along the left subcostal margin. These intrinsic differences may implications for the quality of diagnostic cardiac MRI.[9]

At present, little is known regarding the typical patterns of DRA and image quality in patients with S-ICD and CRT-D, compared to conventional TV-ICD systems when using a standard LGE and WB LGE pulse sequences, although a recent study has shown a

high prevalence of artifact with S-ICD patients, which was reduced by using a WB LGE approach.[9]

Thus, the purpose of this study was to systematically evaluate the artifact patterns and burden by device type in LGE studies utilizing both standard and WB pulse sequences.

Methods

The study was approved by the Institutional Review Board, and each patient provided informed consent for future use of their images for research prior to the MRI examination.

From our cardiac magnetic resonance repository, we retrospectively identified 113 patients with ICD (48 TV-ICD, 48 CRT-D, and17 S-ICD) who had standard and/or WB LGE images acquired. These patients were referred for cardiac MRI at our institution to evaluate for evidence of myocardial scar from February 2016 to July 2019 to evaluate presence of myocardial scar. Inclusion criteria were: 1) age > 18 years; 2) glomerular filtration rate > 30 mL/min/1.73 m^2 to permit administration of gadolinium-based contrast; 3) ability to tolerate the MRI protocol. Exclusion criteria were: ongoing unstable ventricular arrhythmia, gadolinium allergy, ICD implantation within 30 days of MRI, and abandoned and/or retained leads or suspected lead malfunction and/or fracture. The approach to our screening process and safety algorithm (before, during and after MRI) was compliant with Heart Rhythm Society recommendations.[10] Specifically, pre- and post-MRI device interrogation was performed to ensure stability of ICD parameters and inhibit inappropriate tachyarrhythmia therapies during imaging, with adverse device or clinical events recorded for study purposes. Patients were continuously monitored by an advanced cardiac life support certified nurse and a physician, with continuous electrocardiography and pulse oximetry, and blood pressure assessment every 5 minutes. Clinical data including demographics, ICD manufacturer, and clinical comorbidities were obtained from the medical record. Chest X-ray (CXR) on the day of the MRI was analyzed to obtain the minimum distance between the left ventricle (LV) and the generator in the three cohorts (TV-ICD, CRT-D, and S-ICD). Additionally, generator dimensions and mass were obtained from vendor data.

Image Acquisition

MRI was performed using a 1.5 T scanner (Achieva, Philips) with a five-channel surface coil. The study protocol attempted to optimize image quality by raising the arm above the head on the ipsilateral side of the ICD in an effort to increase the distance between the pulse generator and the heart. The WB LGE protocol modified the standard inversion radiofrequency (RF) pulse bandwidth from the vendor's default of 1.8 kHz setting to a fixed 3.8 kHz, based on previously published works.[11] This modified inversion RF was employed in three MRI pulse sequences: first, in a pre-contrast WB inversion RF scout calibration scans to determine the optimal WB RF center frequency shift for minimizing the extent of exhibited device artifacts; second, in a WB LGE Look-Locker T1 scout to determine the optimal inversion time for myocardial nulling, and lastly for WB LGE imaging of the suspected myocardial scar.

Immediately following initial survey views, pre-contrast four- and two-chamber images were acquired using a set of three pre-contrast WB inversion RF calibration scouts obtained at three frequency shifts: −1500, 0, and +1500 Hz. The frequency shift resulting in the lowest DRA was identified for use in the subsequent post-contrast WB LGE sequences. Next, a gadolinium-based contrast agent was administered (Dotarem or Multihance, 0.1–0.2 mmol/kg, according to renal function), and retrospectively gated balanced steady-state free precession short-axis cine images were obtained spanning the LV from base to apex (temporal resolution 25–40 msec). Ten minutes after contrast administration, standard LGE (with 1800 Hz RF bandwidth for the inversion pulse), and/or WB LGE (with 3800 Hz RF bandwidth for the inversion pulse) images acquired in the two-, three-, and four-chamber views, as well as in a short-axis stack of slices.

Both standard and WB-LGE images were acquired using identical T1-weighted gradient-echo acquisition parameters, with typical values as follows: Acquisition matrix = 192 × 192; voxel size: 2 × 2 × 10 mm; TR/TE (repetition time and echo time) = 4.1–4.5/2.0–2.2 msec; default bandwidth per pixel = 479 Hz/pixel; flip angle = 30°; and using SENSE acceleration factor of $R = 2$. Both wideband and standard LGE acquisitions employed phase-sensitive inversion recovery reconstruction. Of note, WB images employed frequency shift value by the pre-contrast calibration scout, and its myocardium nulling time was determined using WB-LL (look-locker) TI scout.

We performed a phantom simulation using extracted (previously in vivo) pulse generators from the three ICD subtypes. Devices were secured to a standard MR phantom and imaged in standard anatomic planes using the set of three pre-contrast WB inversion RF calibration scouts obtained at 3 frequency shifts: −1500, 0, and +1500 Hz. Device artifact position was assessed in the sagittal plane at each frequency shift.

Image Analysis

Image analysis was performed by three independent readers (N.A., A.S., A.R.P.) with 1.5 year, 6 years, and 15 years of CMR experience, respectively. For all patients, the presence or absence of DRA on images obtained using standard LGE and WB LGE was determined by the three readers and recorded in dichotomous fashion. Artifacts were assessed in each short-axis slice for both standard LGE and WB LGE images. Each slice was interrogated for the presence of either examination related artifacts (respiratory motion or “wrap” artifact) or true DRA (off-resonance, signal void, or susceptibility). After artifacts were categorized as device related or “other,” the severity of device-associated artifact was evaluated as follows: from the total short-axis LGE slices, the DRA burden was defined as (the number of short-axis slices exhibiting artifact)/(total number of short-axis slices) × 100% (Fig. 1). The absolute area of artifact involvement in each patient was also quantified as a sum of the area of artifact on all short-axis slices (Fig. 2). Assessment of other artifact burden (including motion or wrap artifact) was additionally calculated using a similar ratio from total short-axis LGE slices, with the burden expressed as a percentage of LGE slices with evidence of non-device-associated artifacts. Presence of LGE was noted by the three independent readers.

Statistical Analysis

After checking for normality using the Shapiro–Wilks test, artifact severity and percentage DRA burden were expressed as a median and interquartile range (IQR), due to non-normal distributions. Continuous baseline clinical characteristics were expressed as either mean and standard deviations or medians and interquartile ranges and categorical baseline clinical characteristics were expressed as frequencies and percentages. Kruskal–Wallis analysis of variance (ANOVA) was employed to determine whether there was a difference in reduction of artifact according to device types for the WB and standard LGE imaging. If the ANOVAs indicated significant differences, Dunn tests with Bonferroni correction were used to determine differences between pairs of device types. Mann–Whitney *U*-tests were used to determine whether there was a significant difference between WB LGE and standard LGE images within each of the three device types. Tests were two-tailed and considered statistically significant for *P*-values <0.05. All statistical analyses were conducted using STATA MP Version 15 (College Station, TX).

Results

Late gadolinium enhancement was frequently encountered in our study patients, with an overall cohort prevalence of 82% determined by WB LGE imaging. Clinical characteristics are shown in Table 1.

On standard LGE imaging, there were more frequent quantitatively severe DRAs impairing image quality in the S-ICD cohort, compared to the other device types. With WB LGE imaging, a negative frequency shift was employed more often in S-ICD patients (41% negative frequency shift), compared to TV-ICD (0% negative frequency shift) where shift selection was either zero or positive, and CRT-D subjects (6% negative frequency shift) (Table 2). Significantly higher artifact burden was noted for S-ICD, compared to either TV-ICD or CRT-D in both LGE sequences (standard LGE: $\chi^2 = 11.84$, $P < 0.05$; WB LGE: $\chi^2 = 29.19$, $P < 0.05$) (Fig. 3). Additionally, the predominant artifact type associated with S-ICD patients was a dark signal void, in contrast to the more frequently encountered hyperenhancement or “off-resonance” artifacts seen in subjects with TV-ICD and biventricular-ICD (Figs. 4 and 5).

When WB LGE imaging was compared to standard LGE imaging, there was a significant reduction in DRA burden for TV-ICD (median [IQR]: 0 [0–7]% vs. 18 [0–50]%, $P < 0.05$). There was a nonsignificant reduction in DRA burden for CRT-D subtypes, and minimal reduction seen for S-CD. (Table 3). Average artifact area was reduced for S-ICD subjects when WB LGE slices were compared to their corresponding standard LGE slices, however (43 ± 28 cm^2 vs. 129 ± 100 cm^2, $P < 0.05$). Assessment of “other artifacts” revealed that CRT-D patients had a statistically significant higher prevalence ($P < 0.05$) of non-device-related artifacts than S-ICD and TV-ICD patients for both standard and WB LGE imaging; the frequency of these non-device-related artifacts in the other ICD subtypes were low (Table 4). We also calculated DRA burden while eliminating slices that had non-device-related artifacts for patients with S-ICD. This calculation resulted in lower DRA burden than when using all slices (Table 3): median 43% (IQR: 11–58).

Measurements from the CXR images showed that the minimum distance between the LV and the device generators (Fig. 6), were not significantly different between the three cohorts (Table 5). However, when vendor specific device dimensions were assessed, the S-ICD device generator had a higher volume and mass (70 cm^3, 138 g) compared to the TV-ICD (32 cm^3, 78 g) and CRT-D (34 cm^3, 75 g) generators. In terms of safety, no adverse clinical events were noted. One examination was terminated early due to subjective feeling of warmth by the patient with a TV-ICD, without detectable changes in device parameters.

Our simulation of the baseline artifact and pattern using a phantom showed that a positive frequency shift amplified hyperenhancement extent for S-ICD, while a negative frequency shift minimized it, with the opposite finding noted when a CRT-D generator was tested (Fig. 7).

Discussion

The practical need for MRI in patients with implantable non-MR conditional devices spans many common clinical scenarios, including assessment of the etiology of non-ischemic cardiomyopathy by LGE pattern, substrate detection for ventricular arrhythmia ablation procedures, and prognostic stratification for mortality and morbidity across a spectrum of cardiomyopathies.[12–20] Previous studies have also illustrated that there is clinical value in the performance of MRI in patients with a range of cardiac implantable electronic devices, resulting in an altered diagnosis in up to 16% of patients and a change in management in 83% of patients.[21] The advancements made in demonstrating both general safety and clinical utility of MRI in patients with ICDs over the last several years have helped to secure its role as an important diagnostic tool, as well as garner recognition for reimbursement by payer groups. However, to do these examinations successfully in these patients, adoption of WB LGE imaging is recommended and perhaps should be considered as the only appropriate LGE imaging sequence, since standard LGE sequences are often fraught with artifacts.

This study expands upon what is known regarding MRI in S-ICD patients by examining the artifact patterns associated with S-ICD devices in LGE imaging compared to other ICD types. Previous work has outlined the feasibility of imaging patients with S-ICDs in general MRI examinations, with a case report describing the application of a WB LGE protocol in a patient with S-ICD, and a more recent study outlining the overall safety and clinical utility in this population.[9, 22, 23] In particular, a study by Holtstiege et al, evaluated the efficacy of multiple pulse sequences in S-ICD subjects for comprehensive aortic and left ventricular perfusion, function, and LGE imaging and found WB LGE did reduce artifact in 65% of subjects.[9] Our study sought to expand upon this important work by systemically quantifying DRA in S-ICD subjects and comparing to other more commonly encountered ICD subtypes. We found that while it is feasible to perform cardiac MRI in patients with S-ICDs, artifacts remain highly prevalent.

Although WB LGE imaging substantially reduced the size of the artifact in S-ICD subjects, DRA was still present in 60% of WB LGE short-axis slices, and thus remained prevalent on imaging. Furthermore, S-ICD related artifacts appeared to be of a different characteristic profile, implying that WB LGE protocols alone may not provide definitive resolution

of artifacts in patients with these devices. S-ICD artifacts with both standard and WB LGE imaging manifested more often as a signal void, as compared to the conventional hyperenhancement associated with off-resonance effects of ICDs. Our findings illustrate the now established observation that WB LGE imaging can eliminate significant device artifact in TV-ICD, but the diminished effect of WB LGE imaging in CRT-D subjects is also noteworthy. In our cohort, the CRT-D patients also had the largest burden of other (non-device-associated) artifacts which may reflect that overall imaging quality in our cohort was not optimal.

Previous reasons postulated for device-related artifacts have invoked the proximity of the device to cardiac structures; in our cohort, CXR analysis showed that there were no significant differences in the minimal distance between the generator of the ICD and the heart border for all ICD subtypes. However, the characteristics of the generator itself could prove an important determinant of artifact burden and pattern, with S-ICD device generators being characterized by higher volume and mass. We additionally noted that the selected frequency shift for WB LGE acquisition in S-ICD patients was negative in 41% of cases, but was never negative for TV-ICD or CRT-D subjects. Given these initial observations, we postulate that further investigation with phantom based imaging could help to understand and predict variations in optimal WB frequency shift and bandwidth depending upon ICD subtype, but this was beyond the scope of our study.

Our findings support the use of WB imaging in patients with non-MRI conditional ICDs. In our analysis, WB LGE sequence perform extremely well in TV-ICD, but have a reduced impact on imaging quality for S-ICD and CRT-D patients. For our CRT-D patients, this may be partly explained by an undue burden of imaging related artifacts including motion, and wrap artifacts. For S-ICD subjects, however, this appeared to primarily be related to the device itself. The patterns of artifact seen with S-ICD are unique with incomplete reductions achieved by using WB LGE imaging. As the implantation of S-ICD devices continues to rise, the ability to evaluate their associated cardiomyopathies and permit performance of MRI examinations will result in increased need for knowledge of how to optimize these examinations of these patients.

Limitations

This was a single-center study that included a relatively small number of S-ICD patients, and not all patients had both standard and WB LGE data to compare for reductions of device artifact. This was in part due to the fact that as our clinical experience using our WB LGE protocol grew, we recognized that standard LGE sequences did not improve the diagnostic utility of the examination, and proceeding directly to WB LGE imaging shortened scan time without compromising image quality, which was advantageous to patient care. However, it is unlikely the final conclusions would be altered even if all patients had both LGE approaches performed. Additionally, while we did not note a significant difference between the distance of pulse generator from the heart border on CXR imaging, this estimated distance is somewhat extrapolated as positioning in the MR scanner involves the patient being supine and often with an ipsilateral arm associated with the ICD site.

Conclusions

The use of WB protocols provided only a modest non-significant reduction in S-ICD associated device artifacts, but performed better for more conventional transvenous ICD systems. Further developments are needed to resolve the artifacts associated with S-ICDs.

Acknowledgments

A.R.P., K.K., H.P. received research support from Philips; H.P. is also supported by National Institutes of Health Grant 2T32HL007381–41A1.

References

1. Russo RJ, Costa HS, Silva PD, et al. Assessing the risks associated with MRI in patients with a pacemaker or defibrillator. N Engl J Med 2017; 376(8):755–764. [PubMed: 28225684]
2. Seewoster T, Löbe S, Hilbert S, et al. Cardiovascular magnetic resonance imaging in patients with cardiac implantable electronic devices: Best practice and real-world experience. Europace 2019;21(8):1220–1228. [PubMed: 31131393]
3. Do DH, Eyvazian V, Bayoneta AJ, et al. Cardiac magnetic resonance imaging using wideband sequences in patients with nonconditional cardiac implanted electronic devices. Heart Rhythm 2018;15(2): 218–225. [PubMed: 29017930]
4. Hilbert S, Jahnke C, Loebe S, et al. Cardiovascular magnetic resonance imaging in patients with cardiac implantable electronic devices: a device-dependent imaging strategy for improved image quality. Eur Heart J Cardiovasc Imaging 2018;19(9):1051–1061. [PubMed: 29048460]
5. Samar H, Yamrozik JA, Williams RB, et al. Diagnostic value of MRI in patients with implanted pacemakers and implantable cardioverter-defibrillators across a cross population: Does the benefit justify the risk? A proof of concept study. JACC Clin Electrophysiol 2017;3(9): 991–1002. [PubMed: 29759724]
6. Singh A, Kawaji K, Goyal N, et al. Feasibility of cardiac magnetic resonance wideband protocol in patients with implantable cardioverter defibrillators and its utility for defining scar. Am J Cardiol 2019;123(8): 1329–1335. [PubMed: 30739658]
7. Stevens SM, Tung R, Rashid S, et al. Device artifact reduction for magnetic resonance imaging of patients with implantable cardioverter-defibrillators and ventricular tachycardia: Late gadolinium enhancement correlation with electroanatomic mapping. Heart Rhythm 2014;11(2): 289–298. [PubMed: 24140812]
8. Kamp NJ, Al-Khatib SM. The subcutaneous implantable cardioverter-defibrillator in review. Am Heart J 2019;217:131–139. [PubMed: 31654943]
9. Holtstiege V, Meier C, Bietenbeck M, et al. Clinical experience regarding safety and diagnostic value of cardiovascular magnetic resonance in patients with a subcutaneous implanted cardioverter/defibrillator (S-ICD) at 1.5 T. J Cardiovasc Magn Reson 2020;22(1):35. [PubMed: 32418537]
10. Indik JH, Gimbel JR, Abe H, et al. 2017 HRS expert consensus statement on magnetic resonance imaging and radiation exposure in patients with cardiovascular implantable electronic devices. Heart Rhythm 2017;14(7):e97–e153. [PubMed: 28502708]
11. Rashid S, Rapacchi S, Vaseghi M, et al. Improved late gadolinium enhancement MR imaging for patients with implanted cardiac devices. Radiology 2014;270(1):269–274. [PubMed: 24086074]
12. Okada DR, Miller J, Chrispin J, et al. Substrate spatial complexity analysis for the prediction of ventricular arrhythmias in patients with ischemic cardiomyopathy. Circ Arrhythm Electrophysiol 2020;13:e007975. [PubMed: 32188287]
13. Elming MB, Hammer-Hansen S, Voges I, et al. Myocardial fibrosis and the effect of primary prophylactic defibrillator implantation in patients with non-ischemic systolic heart failure-DANISH-MRI. Am Heart J 2020; 221:165–176. [PubMed: 31955812]
14. Freitas P, Ferreira AM, Arteaga-Fernández E, et al. The amount of late gadolinium enhancement outperforms current guideline-recommended criteria in the identification of patients with

hypertrophic cardiomyopathy at risk of sudden cardiac death. J Cardiovasc Magn Reson 2019; 21(1):50. [PubMed: 31412875]

15. Guler TE, Yalin K, Aksu T, et al. Prognostic value role of radiofrequency lesion size by cardiac magnetic resonance imaging on outcomes of ablation in patients with ischemic scar-related ventricular tachycardia: A single center pilot study. Medicine 2018;97(46):e12955. [PubMed: 30431569]
16. Mahida S, Sacher F, Dubois R, et al. Cardiac imaging in patients with ventricular tachycardia. Circulation 2017;136(25):2491–2507. [PubMed: 29255125]
17. Siontis KC, Kim HM, Sharaf Dabbagh G, et al. Association of preprocedural cardiac magnetic resonance imaging with outcomes of ventricular tachycardia ablation in patients with idiopathic dilated cardiomyopathy. Heart Rhythm 2017;14(10):1487–1493. [PubMed: 28603002]
18. McLellan AJA, Ellims AH, Prabhu S, et al. Diffuse ventricular fibrosis on cardiac magnetic resonance imaging associates with ventricular tachycardia in patients with hypertrophic cardiomyopathy. J Cardiovasc Electrophysiol 2016;27(5):571–580. [PubMed: 26840595]
19. Njeim M, Yokokawa M, Frank L, et al. Value of cardiac magnetic resonance imaging in patients with failed ablation procedures for ventricular tachycardia. J Cardiovasc Electrophysiol 2016;27(2): 183–189. [PubMed: 26445386]
20. Dixit S, Han Y. Cardiac imaging to define infarct transmurality and guide ventricular tachycardia ablation strategy in patients with ischemic cardiomyopathy. Heart Rhythm 2016;13(1):96–97. [PubMed: 26253037]
21. Bhuva AN, Kellman P, Graham A, et al. Clinical impact of cardiovascular magnetic resonance with optimized myocardial scar detection in patients with cardiac implantable devices. Int J Cardiol 2019;279: 72–78. [PubMed: 30642645]
22. Keller J, Neuzil P, Vymazal J, et al. Magnetic resonance imaging in patients with a subcutaneous implantable cardioverter-defibrillator. Europace 2015;17(5):761–766. [PubMed: 25687749]
23. Rahsepar AA, Collins JD, Knight BP, Hong KP, Carr JC, Kim D. Wideband LGE MRI permits unobstructed viewing of myocardial scarring in a patient with an MR-conditional subcutaneous implantable cardioverter-defibrillator. Clin Imaging 2018;50:294–296. [PubMed: 29747127]

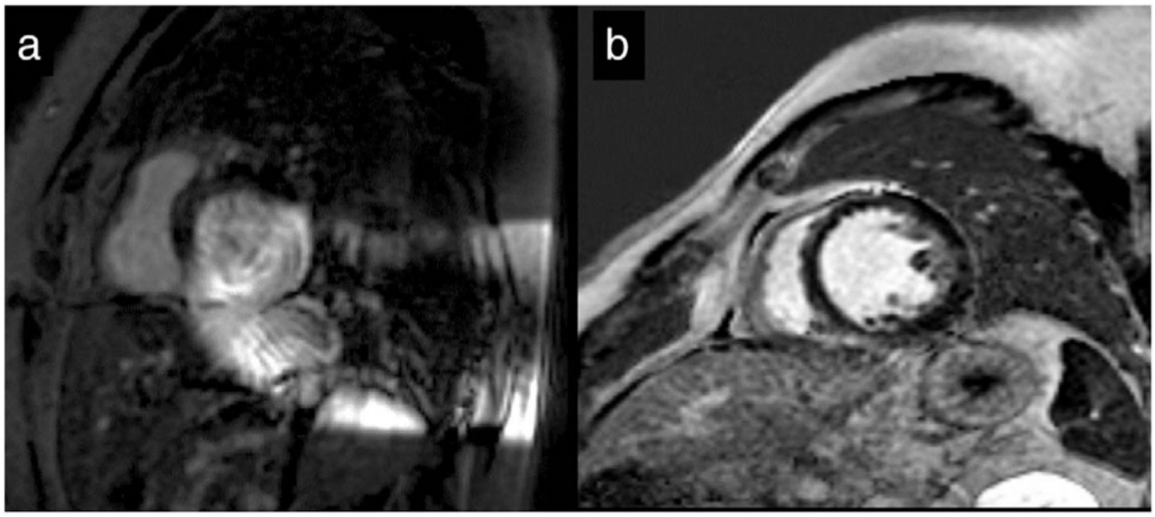

FIGURE 1:
Residual device-related artifact (DRA) in two patients following the use of wideband (WB) late gadolinium enhancement (LGE) protocol. (a) High residual burden DRA in S-ICD subject. Ten of 14 slices affected with DRA 71%. (b) No residual DRA in CRT-D subject. In comparison, WB imaging eliminated the DRA in all 15 slices, resulting in a DRA burden of 0%. CRT-D = cardiac resynchronization therapy device; ICD = implantable cardioverter-defibrillator; S-ICD = subcutaneous ICD.

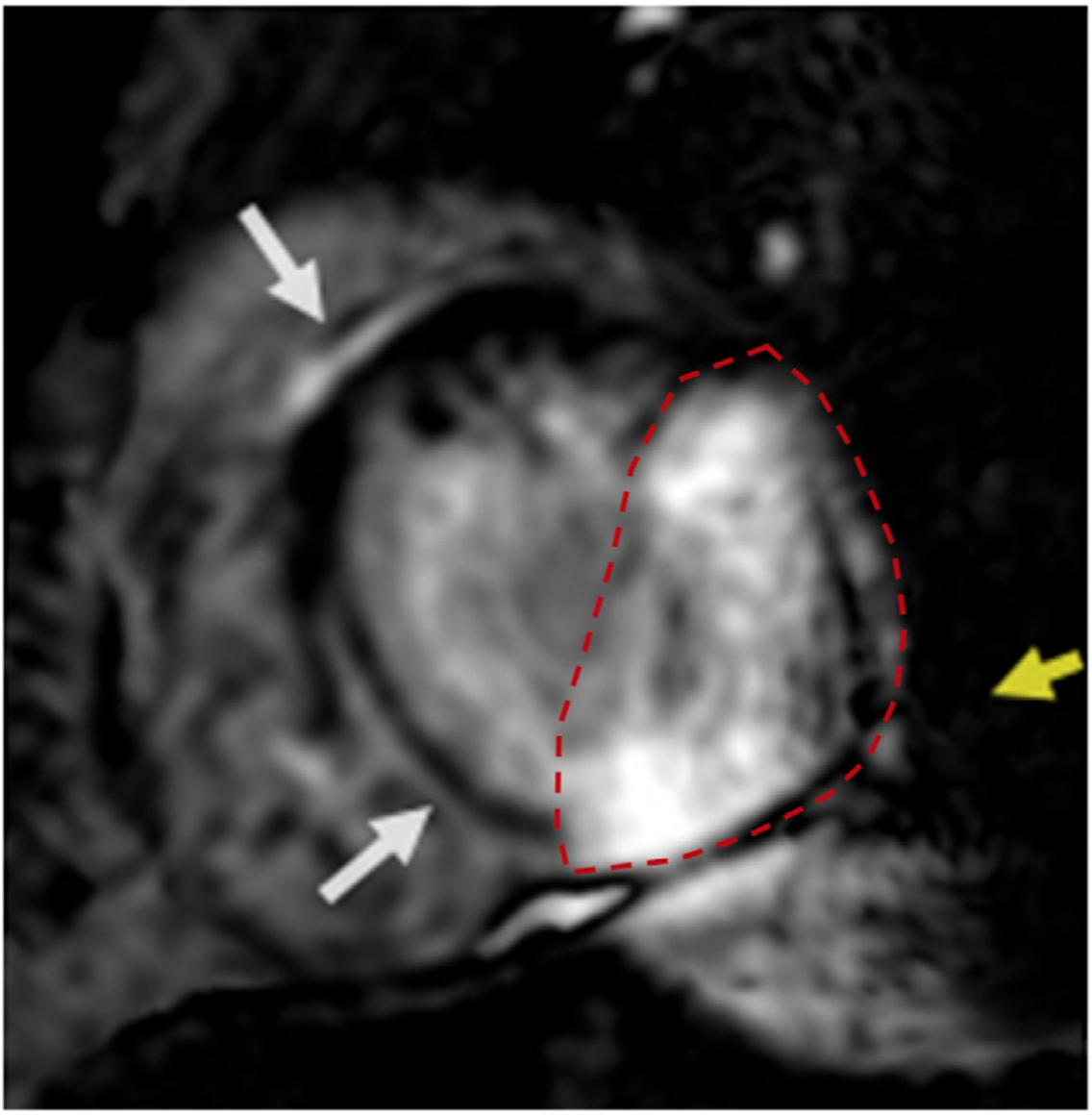

FIGURE 2:
Example of area of artifact estimation on an individual short-axis slice obtained using wideband late gadolinium enhancement (LGE) imaging in a patient with an S-ICD. (Dotted red line indicates the area of artifact; yellow arrow indicates mild signal void artifact; white arrows indicate mid septal LGE). ICD =implantable cardioverter-defibrillator; S-ICD = subcutaneous ICD.

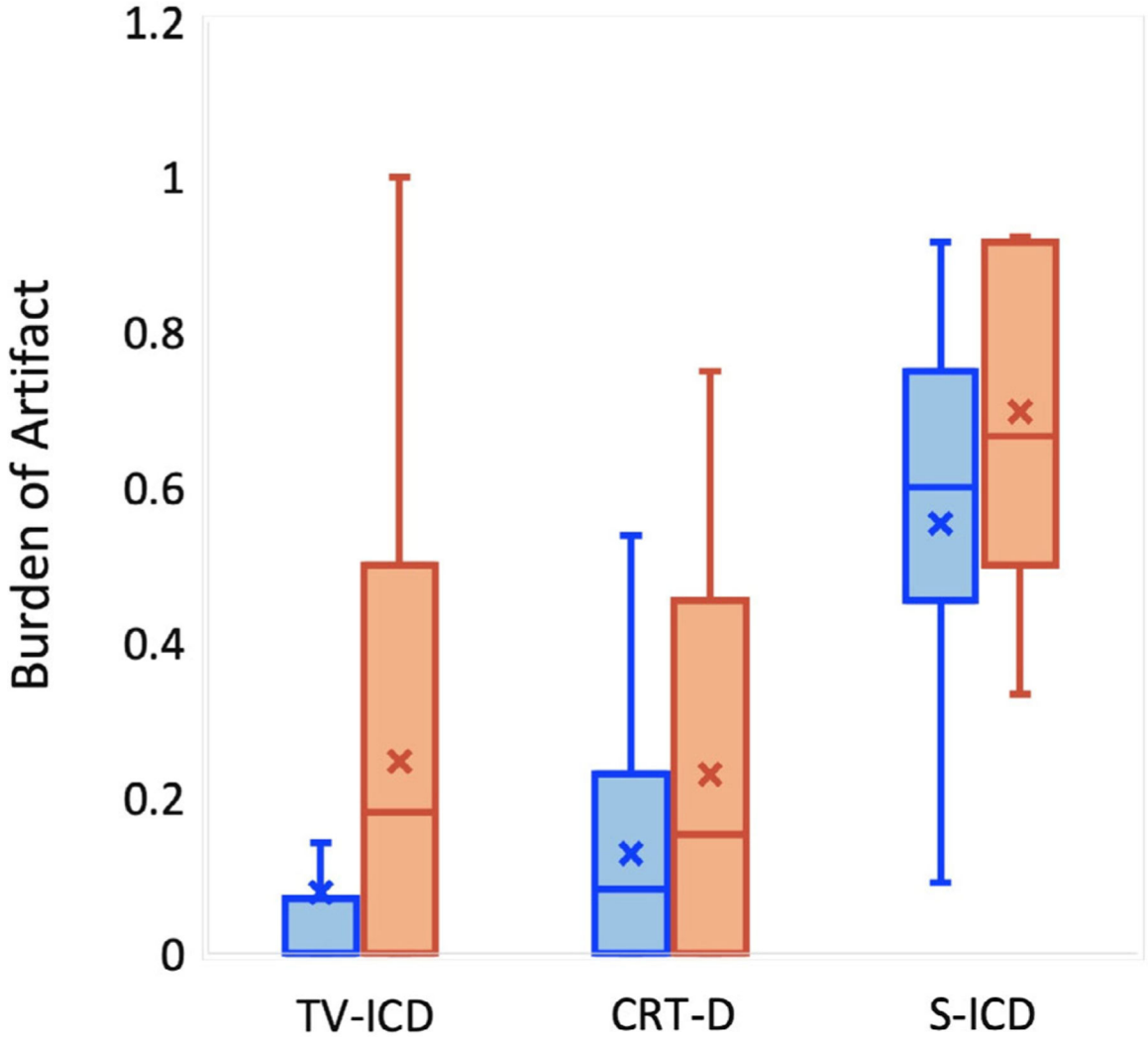

FIGURE 3:

Device-related burden of artifact (%) defined as the number of short-axis late gadolinium enhancement (LGE) slices out of the total number of short-axis slices. Data are presented by implantable cardioverter-defibrillator subtype and LGE sequence (orange = standard LGE, blue = wideband LGE): X indicates mean; bar line indicates median.

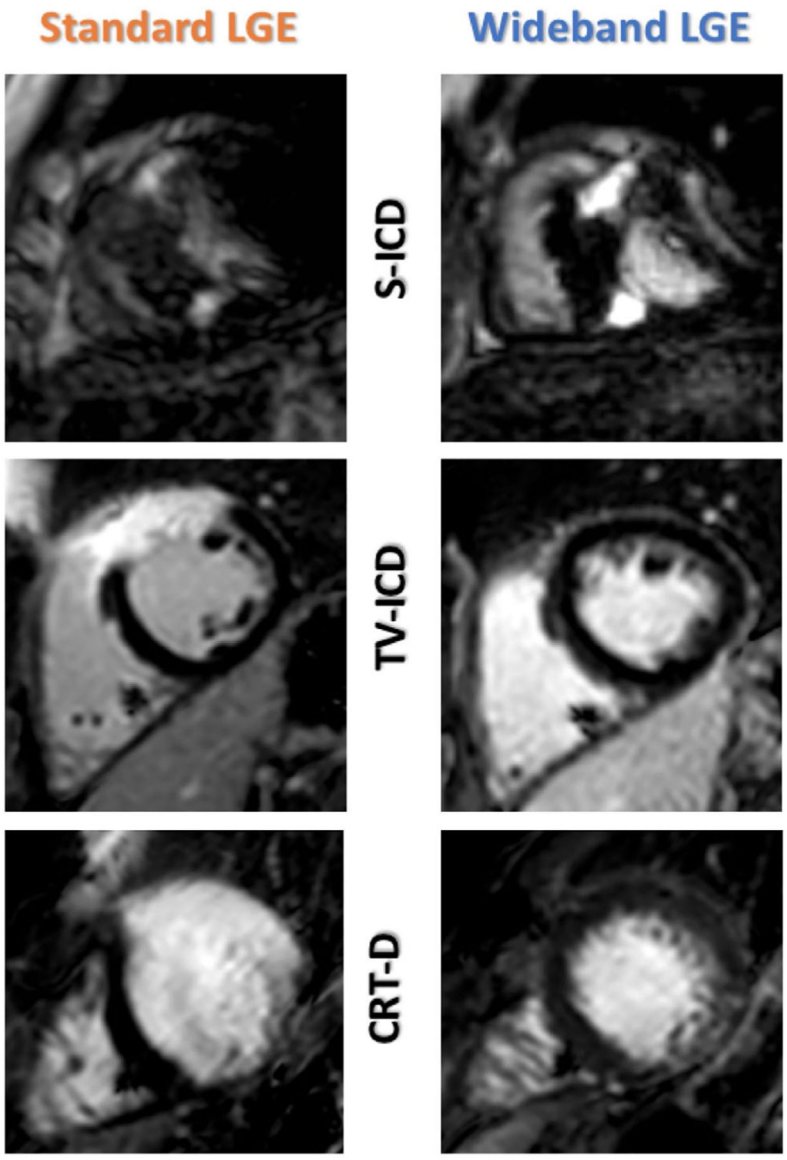

FIGURE 4:
Representative examples of device-related artifact by device type. S-ICD demonstrates a more predominant signal void (top) artifact pattern. ICD = implantable cardioverter-defibrillator; S-ICD = subcutaneous ICD.

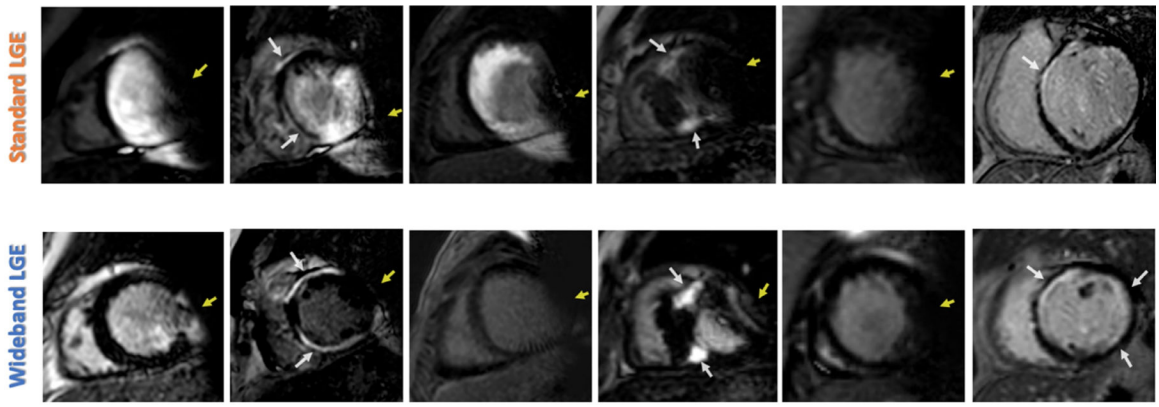

FIGURE 5:
Examples of hyperenhancement and device-related artifacts (DRA) on standard late gadolinium enhancement (LGE) imaging (upper row) and change with wideband imaging (bottom row) in six different patients with a subcutaneous implantable cardioverter-defibrillator. DRA (yellow arrows), LGE (white arrows).

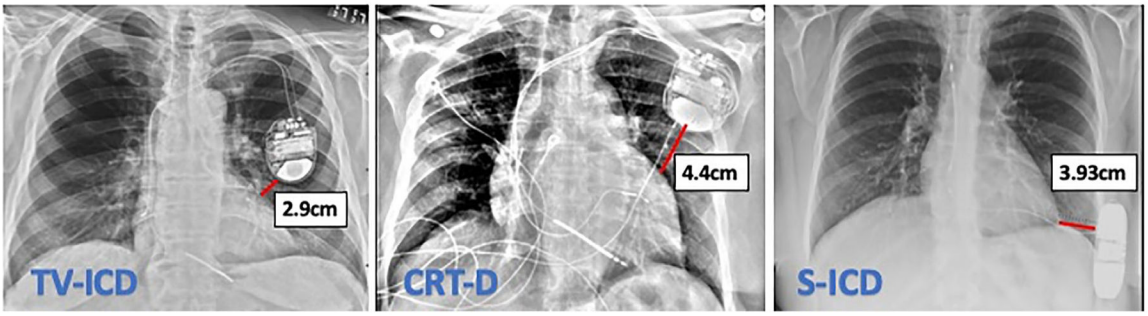

FIGURE 6:
Illustrative example of measurement of device generator distance from the left ventricle in the three patient cohorts.

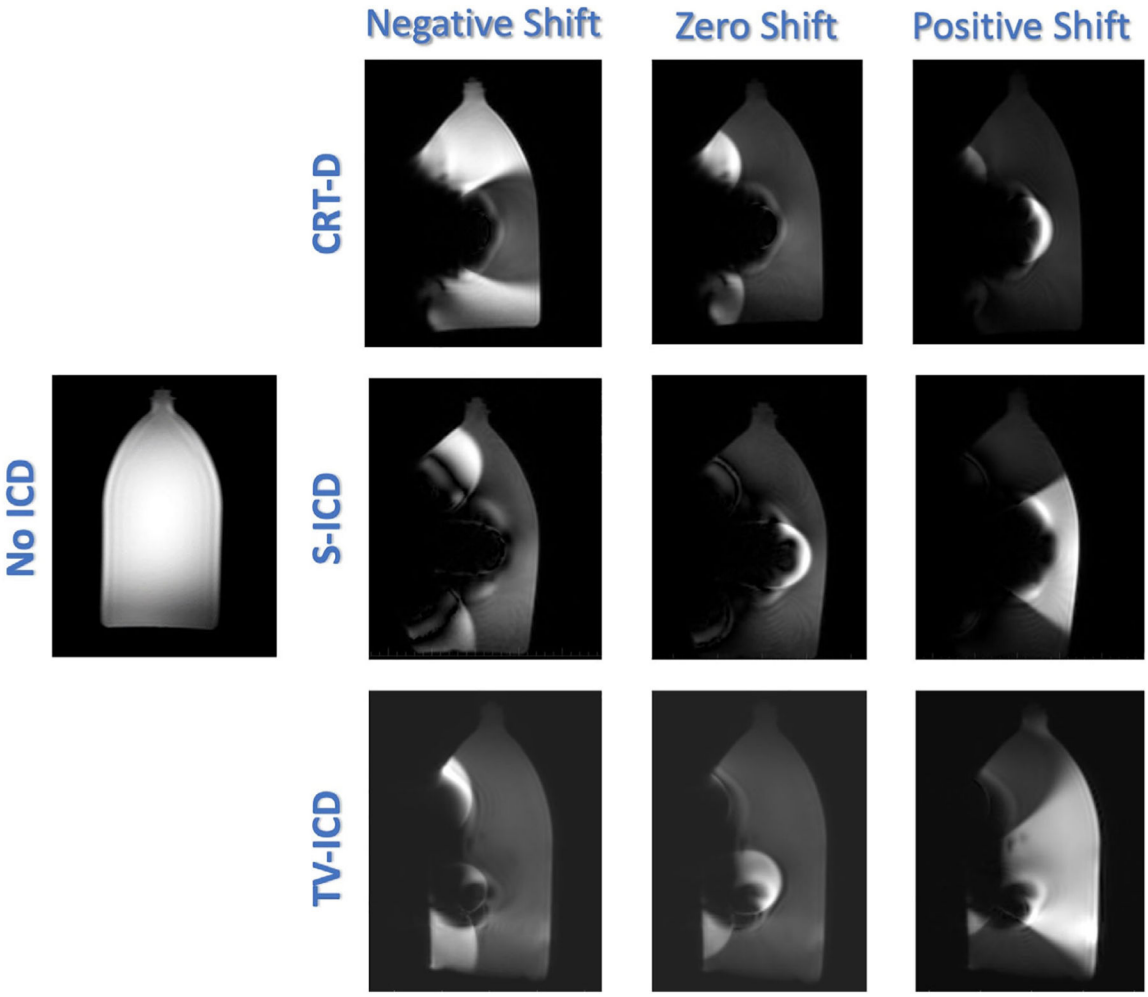

FIGURE 7:
Example of wideband protocol with different phase shifts (positive, zero, and negative) and resultant device artifact using a phantom model with the CRT-D (top), S-ICD (middle), and TV-ICD (bottom) devices. Phantom image without the device is shown on the left for comparison. CRT-D = cardiac resynchronization therapy device; ICD = implantable cardioverter-defibrillator; S-ICD = subcutaneous ICD; TV-ICD = transvenous ICD.

TABLE 1.

Baseline Clinical Characteristics (113 Subjects)

	N **(%)**
Age (years)	63 (50–68)
Male gender	83 (73.5%)
Caucasian	74 (66.7%)
Black	33 (29.7%)
Other	4 (3.6%)
Body mass index (kg/m^2)	29.1 ± 5.4
Hypertension	71 (62.8%)
Diabetes mellitus	35 (31.0%)
Chronic kidney disease	37 (32.7%)
Coronary artery disease	53 (46.9%)
Diagnosis of heart failure	98 (87%)
LV ejection fraction (%)	30 (24–45)
LV end diastolic volume index (mL/m^2)	113 (96–153)
LV end diastolic volume (mL)	246 (194–320)
LV end systolic volume index (mL/m^2)	78 (52.5–120)
LV end systolic volume (mL)	164 (105.5–249.5)
LV mass index (g/m^2)	71 (63–89.5)
LV mass (g)	156 (121–196)

LV = left ventricular.

TABLE 2.

Individualized Frequency Shift Selection for Wideband (WB) Late Gadolinium Enhancement (LGE) Sequences by Implantable Cardioverter-Defibrillator (ICD) Subtype—Comparison of Frequency Shift Selection for Individual Patient WB LGE Examinations

	Negative Shift	Zero Shift	Positive Shift
S-ICD	7/17 (41%)	6/17 (35%)	4/17 (23%)
CRT-D	3/48 (6%)	16/48 (33%)	29/48 (60%)
TV-ICD	0/48 (0%)	13/48 (27%)	35/48 (73%)

TV-ICD = transvenous ICD; CRT-D = cardiac resynchronization therapy device; S-ICD = subcutaneous ICD.

TABLE 3.

Comparison of Device-Related Artifact on Late Gadolinium Enhancement (LGE) Sequences by Implantable Cardioverter-Defibrillator (ICD) Subtype

	WB LGE DRA (%)		Standard LGE DRA (%)		
	Median (IQR)	***N***	**Median (IQR)**	***N***	***P*-Value**
TV-ICD	0 (0–7)[a,c]	48	18 (0–50)[d,f]	47	0.001
CRT-D	8 (0–23)[b,c]	48	16 (0–45)[e,f]	14	0.12
S-ICD	60 (15–71)[a,b]	17	67 (50–92)[d,e]	7	0.09

Device-related artifact (DRA; hyperenhancement or signal void) expressed as a percentage of short-axis slices affected by artifact out of the total number of short-axis slices.

TV-ICD = transvenous ICD; CRT-D = cardiac resynchronization therapy device; S-ICD = subcutaneous ICD; IQR = interquartile range; WB = wideband.

[a] *P*-value for S-ICD versus TV-ICD for WB: $P < 0.001$.

[b] *P*-value for S-ICD versus CRT-D for WB: $P < 0.001$.

[c] *P*-value for TV-ICD versus CRT-D for WB: $P = 0.050$.

[d] *P*-value for S-ICD versus TV-ICD for Standard LGE: $P = 0.001$.

[e] *P*-value for S-ICD versus CRT-D for Standard LGE: $P = 0.006$.

[f] *P*-value for TV-ICD versus CRT-D for Standard LGE: $P = 1.00$.

TABLE 4.

Comparison of Other Imaging Artifact Burden on Late Gadolinium Enhancement (LGE) Sequences by Implantable Cardioverter-Defibrillator (ICD) Subtype

	WB Other Artifact (%)		Standard LGE Other Artifact (%)		
	Median (IQR)	***N***	**Median (IQR)**	***N***	***P*-value**
TV-ICD	0 (0–18)[a,c]	48	7 (0–21)[d,f]	47	0.43
CRT-D	23 (8–33)[b,c]	48	24 (10–33)[e,f]	14	0.73
S-ICD	0 (0–10)[a,b]	17	0 (0–7)[d,e]	7	0.71

As in Table 2, other non-device-related artifact (motion or wrap) is expressed as a percentage of short-axis slices affected by artifact out of the total number of short-axis slices.

TV-ICD = transvenous ICD; CRT-D = cardiac resynchronization therapy device; S-ICD = subcutaneous ICD; IQR = interquartile range; WB = wideband.

[a] S-ICD versus TV-ICD for WB: $P < 0.001$.

[b] S-ICD versus CRT-D for WB: $P = 0.07$.

[c] TV-ICD versus CRT-D for WB: $P = 0.10$.

[d] S-ICD versus TV-ICD for Standard LGE: $P = 0.004$.

[e] S-ICD versus CRT-D for Standard LGE: $P = 0.02$.

[f] TV-ICD versus CRT-D for Standard LGE: $P = 0.19$.

TABLE 5.

Average Minimum Distance from Device Generator to the Left Ventricle on Chest X-ray (Expressed as Average Distance and Standard Deviation)

	Distance (cm)
TV-ICD	3.23 ± 2.9
CRT-D	3.62 ± 2.8
S-ICD	3.62 ± 1.3

P-value nonsignificant for all comparisons.

TV-ICD = transvenous ICD; CRT-D = cardiac resynchronization therapy device; S-ICD = subcutaneous ICD; ICD = implantable cardioverter-defibrillator.